Oscillations of a particle-laden fountain

Chaimae Alaoui, Aurélien Gay, Valérie Vidal

Oscillations of a particle-laden fountain

Chaimae Alaoui[1], Aurélien Gay[2], Valérie Vidal[1]
[1] *ENSL, CNRS, Laboratoire de Physique, F-69342 Lyon, France*
[2] *Géosciences Montpellier, Université de Montpellier, CNRS, Université des Antilles, F-34095 Montpellier, France*
(Dated: August 18, 2022)

Different regimes are usually observed for fluid migration through an immersed granular layer. In this work, we report a puzzling behavior when injecting water at a constant flow rate through a nozzle at the bottom of an immersed granular layer in a Hele-Shaw cell. In a given range of parameters (granular layer height and fluid flow-rate) the granular bed is not only fuidized, but the particle-laden jet also exhibits periodic oscillations. The frequency and amplitude of the oscillations are quantified. The Strouhal number displays a power-law behavior as a function of a non-dimensional parameter, J, defined as the ratio between the jet velocity at the initial granular bed height and the inertial particle velocity. Fluid-particle coupling is responsible for the jet oscillations. This mechanism could be at the origin of the cyclic behavior of pockmarks and mud volcanoes in sedimentary basins.

I. INTRODUCTION

Particles entrained by fluid motion are not only a fascinating topic for physicists, but are also at the core of present-day challenges in geosciences or in industrial processes. Fluid migration in sedimentary basins and their subsequent expulsion at the seafloor lead either to gentle fluid release and the formation of pockmarks [1, 2], or to violent subsea fluid release such as mud volcanoes [3]. These latter can exhibit puzzling periodic behaviors [4]. In spite of modeling attempts [5], the underlying mechanism for this cyclicity is still unknow but could provide keys for predicting these phenomena and improve hazard mitigation. In the industrial context, fluidized beds are classically used in heterogeneous catalysis to enhance multiphase reactions [6, 7]. However, the emergence of instabilities in the suspension may be at the origin of a chaotic behavior of the reactor and potentially dangerous exothermic reactions [8].

Since the work of Ergun & Orning and the first description of a fluid flow through expanded and fluidized beds [9], countless studies have focused on the complex problem of particle entrainment by fluid flows in different configuration. Examples include, in a non-exhaustive way, submarine avalanches [10], erosion processes [11, 12], crater formation [13, 14] or bedload transport [15, 16]. The complexity of such flows, involving a strong coupling between the particles and the fluid, hydrodynamics and contact interactions, transport and sedimentation, bring forward numerous challenges for the physicists including finding a constitutive equation and the rheology of dense packings [17], quantifying the role of pore pressure and lubrication forces [18, 19], friction and particle roughness [20] and compaction [21].

In practical applications, either natural or industrial, a localized fluid injection is the source of the system dynamics. In other words, the system can be described as the injection of the fluid through a single orifice at the base of an initially sedimented granular bed. Theoretical, numerical and experimental studies have thoroughly investigated this configuration for two-phase flows [22–27]. Different invasion regimes are reported when the injected flow-rate increases: fluid percolation through a static bed, formation of a stable fluidized cavity which does not reach the grannular bed surface, or fluidization over the entire granular layer height. However, to our knowledge, no previous work has described the dynamics of the particle-laden jet inside the fluidized zone.

In a recent work, Vessaire *et al.* investigated a liquid jet impinging on a confined saturated granular bed [28]. This configuration unraveled a puzzling phenomenon: in a given range of parameters, the jet is strong enough to form a crater containing suspended particles and exhibits oscillations. Although apparently different, this downward particle-laden jet is strongly reminiscent of the upward particle-laden jet reported for localized fluidization when injecting a fluid at the base of a granular layer.

The present work investigates the dynamics of the particle-laden jet formed after the onset of localized fluidization when injecting water at constant flow rate through a single nozzle at the base of an immersed granular layer. Experiments are performed in a Hele-Shaw cell, which allow a direct visualization (Sec. II). We report the emergence of periodic oscillations and characterize their existence (Sec. III), frequency and amplitude (Sec. IV). Finally, we discuss the results in comparison to the impinging jet configuration, and other types of hydrodynamic instabilities (Sec. V).

II. EXPERIMENTAL SETUP

Experiments are performed in a Hele-Shaw cell, consisting in two glass plates separated by a gap $e = 2$ mm. The cell inner dimensions are 31.5 cm (height) $\times$ 35 cm (width). Initially, the cell is filled with a granular layer up to a height h_g, fully immersed in distilled water (density $\rho_f = 1000$ kg/m^{-3}, viscosity $\eta_f = 10^{-3}$ Pa s). The particles are spherical glass beads (USF Matrasur) of diameter d_p and of density $\rho_p = 2300$ kg/m^{-3}. The density difference between the grains and surrounding fluid is $\Delta\rho = \rho_p - \rho_f = 1300$ kg/m^{-3}. The granular layer

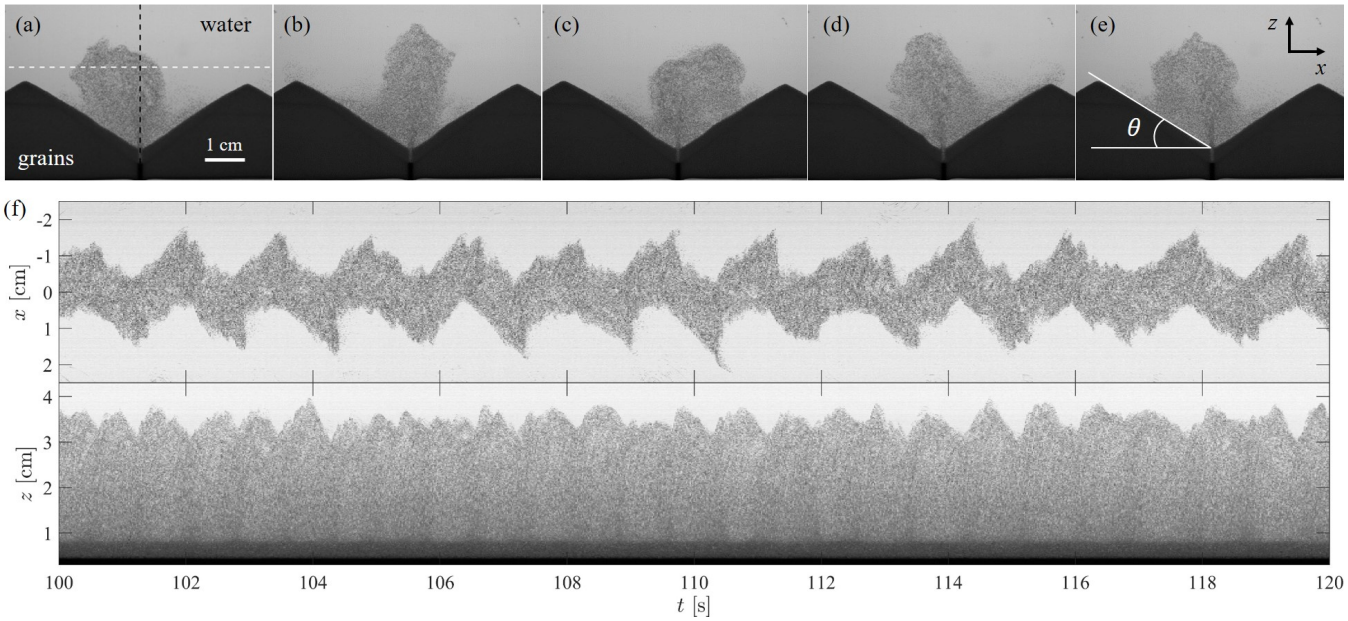

FIG. 1. (a)-(e) Snapshots of the experiment illustrating one period of oscillations of the particle-laden jet ($h_g = 2$ cm, $Q = 35$ mL/min). (a) $t = 103.46$ s; (b) $t = 103.9$ s; (c) $t = 104.3$ s; (d) $t = 104.6$ s; (e) $t = 104.9$ s. Time $t = 0$ corresponds to the valve opening and the fluid entrance from the nozzle (in black at the bottom center of the image). Image (e) indicates the $x-$ and $z-$axes and the inner angle of the crater, θ. (f) Space-time diagrams illustrating the jet oscillations along a horizontal profile [white dashed line in (a) located 2.4 cm above the nozzle, upper panel] and a vertical profile above the injection nozzle [black dashed line in (a), lower panel].

height varies from $h_g = 1$ to 8 cm. Although most experiments have been performed with $d_p = 106 - 212$ μm, additional experiments have also been analyzed with $d_p = 400 - 600$ μm, or with no grains for comparison (see Sec. III).

At time $t = 0$, water is injected at constant flow-rate Q from a nozzle (inner diameter $d_i = 1.1$ mm) located at the bottom center of the cell. A flow-rate controller (Bronkhorst mini CORI-FLOW M14-AAD-22-0-S, $2 - 100$ mL/min) connected to a pump upstream (Bronkhorst Tuthill 7.11.468) made possible to explore a range of flow-rates $Q = [3 - 90]$ mL/min. A transparency flat viewer (Just NormLicht, Classic Line) located behind the cell ensures a homogeneous backlight. Direct visualization of the two-phase system at time $t \geq 0$ is performed by means of a camera CMOS 1" (BASLER acA2040-90um, monochrome, full resolution 2048×2048 pixels) with a lens of focal distance 16 mm, located at about 26 cm from the cell. Calibration with a grid and geometrical corrections are applied (with Matlab software) to account for small optical distorsions on the sides of the image. All experiments are recorded at 50 fps, for a duration of typically 2 min. Reproducibility is checked by performing twice all experiments.

III. DIFFERENT REGIMES

Different regimes are reported for fluid migration in the granular layer and are described in the next paragraph. The most puzzling observation, which is the central part of this work, is reported for $d_p = 106 - 212$ μm in a given range of parameters (Q, h_g). In this range, the upward jet does not only fluidize the granular layer, as already reported in previous works in similar configurations [23–27, 29, 30], but also exhibits periodic oscillations as illustrated in Figure 1. In this regime, after reaching the surface, the particle-laden jet oscillates regularly from one side to the other of the central crater. This latter is formed by the particles suspended by the upward flow and deposited on either side of the crater, in a way similar to crater growth in immersed granular media with gas injection [13]. The jet oscillations develop in a given region of the fluidization regime, for low h_g and above a critical flow-rate (black circles, Figure 2).

A thorough exploration of the parameter phase space (Q, h_g) makes possible to identify the regions associated with the three different regimes. (1) In the percolation regime (white squares, Figure 2), the fluid migrates upward through the granular bed without moving significantly the grains, even if a slight decompaction is observed (see movie 1 [31]). (2) In the fluidization regime (gray triangles, Figure 2), particles are lifted and after a transient, the central region is fluidized and a crater forms with dunes on each side. The particle-laden jet

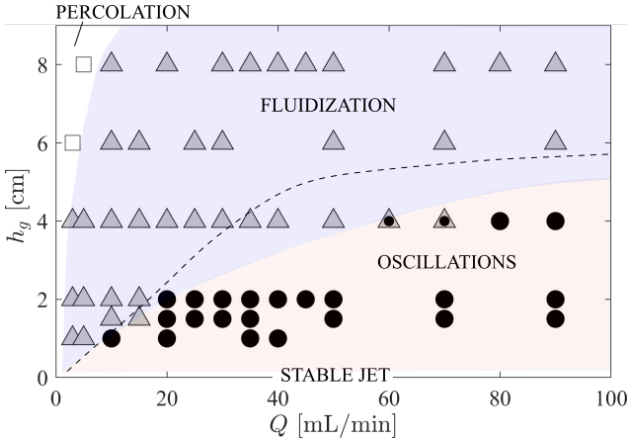

FIG. 2. Different regimes for fluid migration through the granular layer [$d_p = 106-212$ μm]. □ Percolation; △ fluidization; ◯ fluidization with particle-laden jet oscillations (see text). Double symbols for $h_g = 4$ cm, $Q = 60 - 70$ mL/min indicate different regimes observed when repeating the experiment. The colored regions are guides for the eye. The dashed line indicates the limit between percolation and fluidization for $d_p = 400 - 600$ μm (see text). For these largest particles, no oscillations are observed. For $h_g = 0$ (no grains), a stable jet is observed for all flow rates.

fluctuates inside this region but does not exhibit periodic oscillations (see movie 2 [32]). (3) In the oscillations regime, the central region is fluidized and in the stationary regime (see Sec. IV B), the upward jet flaps with a given frequency (Figure 1 and movie 3 [33]). For $h_g = 4$ cm, although oscillations are observed for $Q \geq 60$ mL/min, a variability is reported when repeating the experiments at $Q = 60$ and 70 mL/min. A first set of data displays clear oscillations, whereas a second set of data shows jet fluctuations without any clear periodicity. Although in the following $Q_c = 60$ mL/min will be considered as the critical flow-rate for the emergence of oscillations, these two datasets will not be considered in the jet oscillations analysis (Sec. IV).

For particles of larger diameter ($d_p = 400 - 600$ μm), although a clear transition between the percolation and fluidization regime is reported (dashed line, Figure 2), the oscillation regime is never observed in the explored range of parameters. Experiments have also been performed without grains, injecting the fluid in the Hele-Shaw cell initially filled with the same fluid only. A stable jet is observed for the whole range $Q = 3-90$ mL/min (Figure 2, $h_g = 0$). In the following section, we focus on the oscillating regime of the particle-laden jet ($d_p = 106 - 212$ μm) and quantify the oscillations properties.

IV. JET OSCILLATIONS

A. Data analysis

To quantify the jet oscillations, the experimental data are analyzed as follows. First, images are cropped to keep the central zone only, including the jet, whose maximum vertical extent is, in the stationary regime, higher than the initial granular bed [see Figure 1d for example]. To avoid contour detection problems when the jet has a low particle volume fraction, the computation is based on the difference between two consecutive frames. The image acquisition rate being much larger than the oscillations frequency, it improves the image analysis without introducing a significant error in the jet maximum height detection. After binarization, morphological operations are performed (*imclose, imfill, imfilter* with Matlab software, *MathWorks*®) to identify the largest particle-laden region including both the particles remaining at rest on each side of the crater and the particle-laden jet. Its edges are detected with a Sobel method. The jet maximum point (X_j, Z_j), corresponding to the coordinates of its further extent in the $z-$direction is then obtained as a function of time, for each experimental series.

B. Stationary regime

At the beginning of each experiment in the oscillations regime, the fluid invades the granular layer, migrates upward through local fluidization and reaches the surface, leading to the full fluidization of the granular layer. The particle-laden jet maximum can only be detected after this time, which lasts in average less than 5 s after the first fluid injection. Figure 3 displays the temporal evolution of the jet maximum (X_j, Z_j) for different flow rates. In the transient regime, the jet height Z_j increases until it reaches a plateau, hereafter p_z^*, superimposed with the oscillations (Figure 3b). The amplitude of the oscillations grow during the transient (Figure 3a), until reaching a value A_x^* (along the horizontal, Figure 3a) or A_z^* (along the vertical, Figure 3b).

Figure 4 shows the jet maximum height in the stationary regime, p_z^*, as a function of the imposed fluid flow-rate Q. The jet height is normalized by the initial granular bed thickness, h_g, while the flow-rate is normalized by the critical flow-rate Q_c above which the oscillations appear for each initial granular layer height h_g. For $Q/Q_c \leq 1$, all data collapse to $p_z^*/h_g = 1$. Except small fluctuations, the jet height equals the initial granular layer height, and no oscillations are reported (open symbols, Figure 4). For $Q/Q_c > 1$, the data are scattered but display an increase of the jet height as a function of Q/Q_c. A simple fluid analogy and force balance leads to

$$p_z^* = \frac{v_i^2}{2\left(\frac{\rho_j - \rho_w}{\rho_w}\right) g} \tag{1}$$

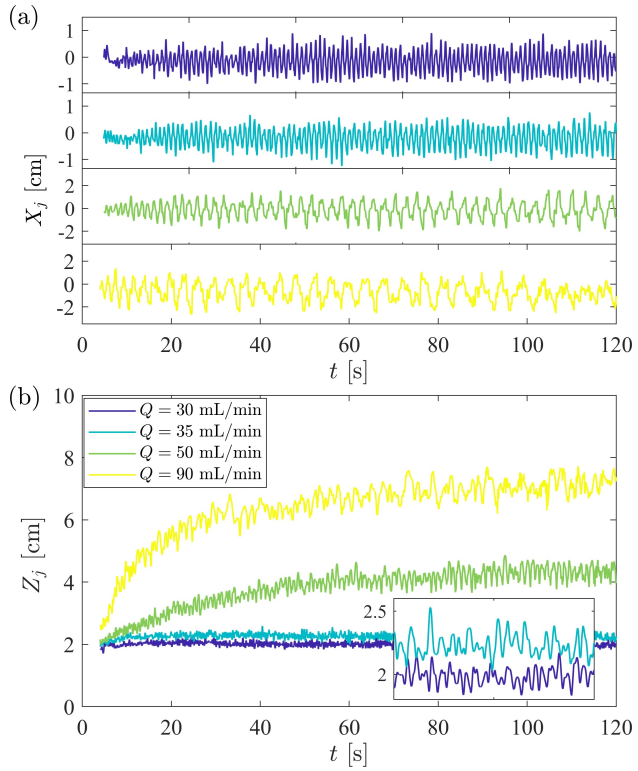

FIG. 3. Temporal evolution of the jet maximum height (a) horizontal position X_j and (b) vertical position Z_j for different flow rates ($h_g = 2$ cm). After a transient, the jet height Z_j reaches a plateau p_z^* superimposed with oscillations. *Inset:* zoom between $t = 110$ and 120 s showing the osillations for the lowest flow-rates.

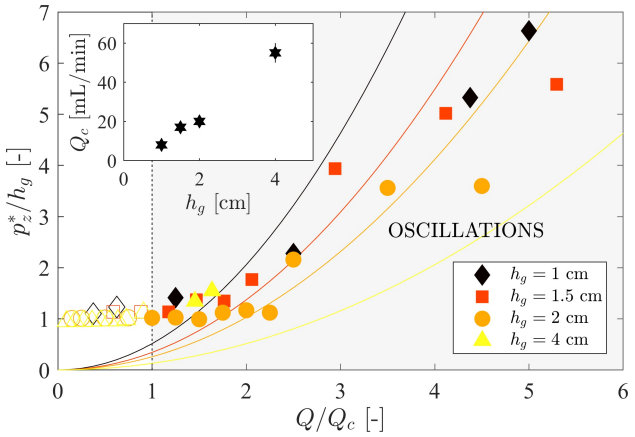

FIG. 4. Normalized jet height p_z^*/h_g in the stationary regime as a function by the normalized flow rate Q/Q_c, where Q_c is the critical fluid flow rate above which oscillations appear, for different initial granular bed height h_g. Open symbols: no jet oscillations; filled symbols: jet oscillations (gray region). The errorbars are smaller than the symbol size. The solid colored lines correspond to the prediction of equation 1 for each h_g. *Inset:* critical flow rate Q_c as a function of h_g.

where $v_i = Q/(\pi d_i^2/4)$ is the initial jet velocity at the nozzle exit and $\rho_j = \phi\rho_p + (1-\phi)\rho_f$ the particle-laden jet density with ϕ its particle volume fraction. Considering $\phi \simeq 15$ % as a reasonable estimate leads to the prediction displayed by the solid lines in Figure 4 for each h_g. Although based on a crude approximation, this prediction captures well the jet height order of magnitude. However, it fails in capturing the granular jet height at low flow-rates (for $Q < Q_c$ in the fluidization regime, $p_z^*/h_g \simeq 1$). This is due to the fact that this simple fluid analogy does not account for the initial granular layer. This latter remains present on both sides of the jet, even after total fluidization, and grains avalanching in the inner part of the crater participate to the jet dynamics, which explains why the jet maximum height does not tend to zero when the flow-rate decreases to zero. Equation 1 also fails in predicting the oscillations, which appear when the jet becomes higher than h_g ($p_z^*/h_g > 1$, filled symbols and gray region, Figure 4).

Note that for $h_g = 1$ cm, we could not detect the jet maximum for $Q > 40$ mL/min due to the very low particle volume fraction inside, resulting in the failure of the image analysis presented in section IV A. When increasing the initial bed height the critical flow rate increases (Figure 4, inset). This is consistent with the fact that the particle-laden jet has to reach a maximum higher that the initial granular layer to undergo oscillations. Henceforth, we focus on the oscillation properties in the stationary regime.

C. Frequency

The jet oscillations frequency along the $x-$ and $z-$axis, respectively f_x and f_z, are computed from the temporal evolution of the jet maximum displayed in Figures 3a,b. First, the mean evolution of Z_j (increase + plateau) is removed from the signal in Figure 3b, so that the oscillatory part with an average at zero is extracted from Z_j. Then spectrograms based on Fast Fourier Transforms are computed. In the stationary regime, the frequencies f_x and f_z are constant and depend on (Q, h_g) only. They are extracted from the spectrograms as the average values over the stationary regime of the spectrogram maximum at each time t. The error on both frequencies estimation is estimated as the standard deviation over the same temporal window.

Figure 5a shows the jet oscillations frequency along z, f_z, as a function of the oscillations frequency along x, f_x, for different h_g (different symbols) when varying the flow rate Q (color filling the symbols, see colorscale on the right part of the figure). When increasing the flow rate, both frequencies decrease. Interestingly, all experimental data collapse on a single curve, $f_z \simeq 2f_x$, whichever the parameters (Q, h_g). This indicates that the particle-laden jet experiences oscillations analog to a solid-body oscillation, reminiscent of a metronome. This result will be further analyzed in the next section IV D. As both quantities are directly proportional, in the following, we

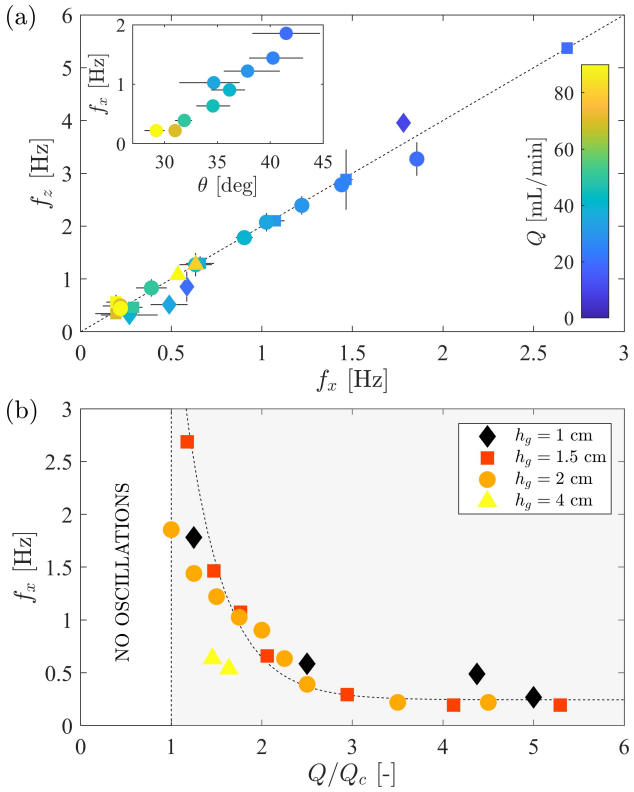

FIG. 5. (a) Oscillation frequency along the $z-$axis, f_z, as a function of the oscillation frequency along the $x-$axis, f_x, for different initial granular height (symbols corresponding to the legend in b). When not visible, the errorbars are smaller than the symbol size. The colorscale indicates the value of the injection flow rate Q. The dashed line indicates $f_z = 2f_x$. *Inset:* f_x as a function of the inner angle θ of the crater (see Figure 1e). (b) Frequency of the jet horizontal oscillations f_x as a function of the normalized flow-rate Q/Q_c for different initial granular height. The dashed line is a guide for the eye.

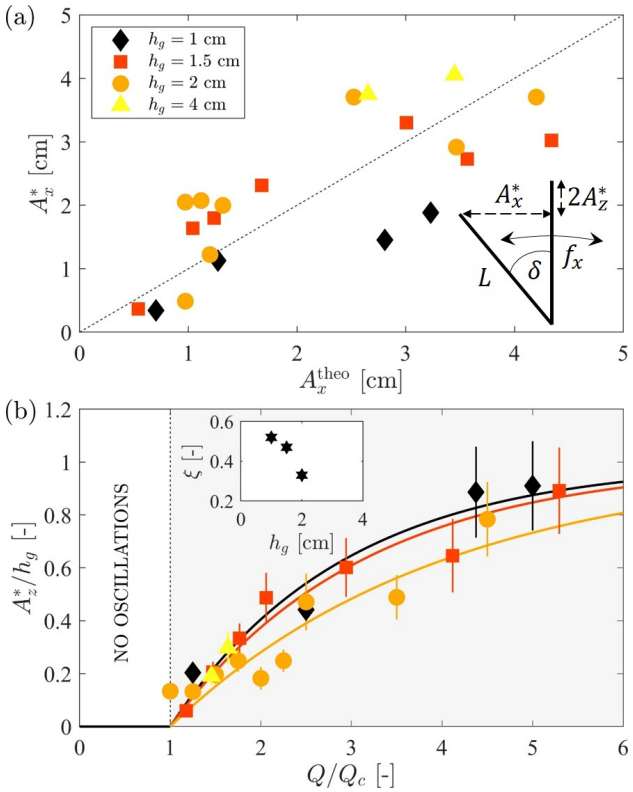

FIG. 6. (a) Amplitude of the jet horizontal oscillations in the steady-state regime, A_x^*, as a function of the amplitude predicted by the metronome model, A_x^{theo} (inset). The dashed line indicates 1:1 relation. (b) Amplitude of the jet vertical oscillations in the steady-state regime, A_z^*, normalized by the initial granular bed height h_g, as a function of the normalized flow-rate Q/Q_c. The colored lines correspond to equation 3 for each data set (see text). Inset: coefficient ξ (equation 3) .

shall only use f_x as the jet characteristic frequency. Figure 5a, inset, displays f_x as a function of the inner angle θ of the central crater formed by the jet (see Figure 1e). The crater angle decreases when increasing the flow rate until reaching for high flow-rate $\theta \simeq 28°$, corresponding to the avalanche angle [13]. The oscillation frequency is directly linked to the crater geometry, f_x being highest for $\theta \simeq 42°$, and decreasing when the crater becomes more open.

Figure 5b displays the horizontal oscillations frequency f_x as a function of the normalized flow-rate Q/Qc. The frequency strongly decreases with the normalized flow-rate until reaching a plateau at about 0.2 Hz. This plateau is attained when the crater angle θ reaches the avalanche angle, $\theta \simeq 28°$. The data roughly collapse on an exponential decay (Figure 5, dashed line as a guide for the eye), with the exception of the two data points at $h_g = 4$ cm.

D. Amplitude

To investigate further the hypothesis of a solid-body oscillation (metronome model), we can estimate theoretically the relationship between the horizontal and vertical amplitudes of oscillations in the steady-state regime, A_x^* and A_z^*, respectively. Figure 6a, inset presents a sketch of the metronome model, with $L = p_z^* + A_z^*$. Simple trigonometry with $A_x^* = L \sin\delta$ and $A_z^* = L/2(1 - \cos\delta)$ leads to the theoretical expression of A_x^* given by

$$A_x^{\text{theo}} = A_z^* \sqrt{2\left(\frac{p_z^*}{A_z^*} - 1\right)}. \qquad (2)$$

From the experimental measurements of p_z^* and A_z^*, A_x^{theo} is computed and compared to its experimental value (Figure 6a). Despite some scattering, both values agree satisfactorily, showing once again the pertinence of the analogy between the jet oscillations and solid-body oscillations.

Figure 6b displays the amplitude variations of the jet vertical oscillations in the steady-state regime, A_z^*, nor-

malized by the initial granular bed height h_g, as a function of the normalized flow-rate Q/Q_c. The vertical oscillations, obviously limited for their maximum amplitude to the value of h_g, grow exponentially for all h_g with the following law when the flow-rate increases:

$$A_z^* = h_g \left(1 - \exp^{-\xi\left(\frac{Q}{Q_c}-1\right)}\right) \quad (3)$$

The coefficient ξ has been determined by a least-squares, trust-region algorithm and is displayed as a function of h_g in Figure 6b, inset. Although it is difficult to be conclusive with only three data points, we observe that ξ decreases with h_g. Note that ξ has not been estimated for $h_g = 4$ cm, which does not allow a proper fit with two data points only. Considering $\xi \simeq 0.4$ as a reasonable approximation, this empirical law makes it possible to predict the jet oscillations amplitude over almost all the experimental range.

V. DISCUSSION

The frequency of the particle-laden jet oscillations can be expressed in a dimensionless form by the Strouhal number $St = fL/u_J^0$ where the characteristic length is $L = h_g$ and $u_J^0 = Q/S_i$ is the jet velocity at the nozzle exit, with $S_i = \pi d_i^2/4$ the surface through which the fluid is injected at the cell bottom. Following [28], we introduce a dimensionless number corresponding to the velocity ratio between the particle-laden jet, u_J, at height h_g and a single grain velocity u. The jet velocity is derived in confined geometry as $u_J \simeq Q/(2eh_g \tan\alpha)$, where e is the cell gap and α the jet half-angle. The inertial particle velocity corrected from buoyancy effects is defined as $u = \sqrt{(\Delta\rho/\rho_f)gd}$, with g the gravitational acceleration. We thus get

$$J = \frac{Q}{(2eh_g \tan\alpha)u}\,. \quad (4)$$

This dimensionless parameter is adapted from the erosion parameter E classically used in the literature [34] for confined geometry. Note that it also corresponds to the square root of a Shields number. Here $\alpha \simeq 7°$, of the order of the value measured by Vessaire *et al.* [28].

Figure 7 displays the Strouhal number St as a function of the parameter J. Similar to the jet impingement configuration [28], all data points collapse on a single curve and St exhibits a power-law behavior, $St = \beta J^\gamma$, with $\beta \simeq 0.06$ and $\gamma \simeq -5/2$. Interestingly, although in both the jet impingement or the upward jet configuration the Strouhal number decreases with J, the exponent of the power-law behavior is drastically different ($\gamma \simeq -1$ in the reverse configuration [28]).

The emergence of jet self-sustained oscillations has been pointed out in previous works as the consequence of a feedback loop, generated either by impingement on an obstacle [35–39] or by a specific nozzle configuration or mixing chamber such as in fluidic oscillators [40, 41].

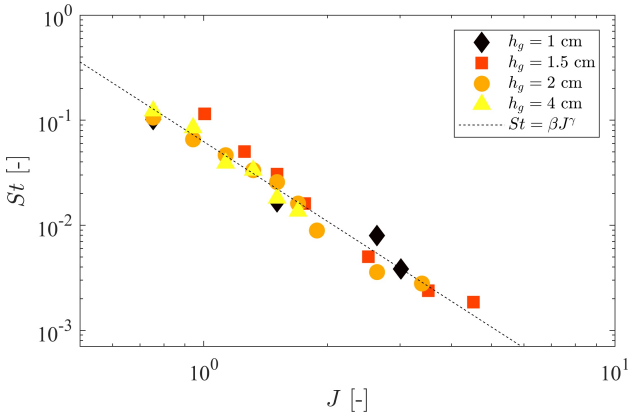

FIG. 7. Strouhal number as a function of the J parameter (see text). The dashed line indicates $St = \beta J^\gamma$ with $\beta \simeq 0.06$ and $\gamma \simeq -5/2$.

One possible mechanism at the origin of the oscillations is hydrodynamic, with structures advected by a recirculation flow and interacting back with the nozzle. In this case, the subsequent oscillations frequency - and thus, the Strouhal number - increases with the jet velocity [37]. Another possible origin for the feedback is the generation of acoustic waves which propagate upstream and interact back with the nozzle. At low Mach numbers, this mechanism is characterized by a constant Strouhal number [42].

Neither the acoustic nor hydrodynamic origin can explain the oscillations frequency of the particle-laden jet reported in this work, as the Strouhal number decreases with the jet speed, with all other parameters being constant for a given initial granular bed height (Eq. 4). Vessaire *et al.*, who also discarded these two mechanisms, proposed that the mechanism at the origin of the decreasing frequency with the jet velocity is a coupling between the fluid and the grains - the jet oscillations in their experiment beeing directly coupled with the crater aperture width oscillations. This argument seems valid for the present observations. First, the oscillation frequency is also linked, in the present configuration, with the crater opening. Then, when the jet is oriented on one side, it entrains particles which fall on the central crater same side (Figure 1 and movie 3, Supplemental Materials). These particles avalanche back toward the injection nozzle, resulting in a flow which pushes the jet base toward the other side, and so on. The lower frequencies found in our experiment ($f_x < 3$ Hz) with respect to the reverse configuration of an impinging jet ($f_x \simeq 3$ Hz [28]) could be explained by the difference in particle size and the resulting crater geometry.

Note that the fluid viscosity does not play any role, as the particle speed in this work is given by the inertial velocity, and only depends on the particle diameter, its density difference with the surrounding fluid and the gravitational acceleration. We expect the jet dynamics to be different in the viscous regime, possibly without

any emergence of instabilities.

VI. CONCLUSION

This work reports the appearance of self-sustained oscillations of a particle-laden jet when injecting water at constant flow-rate at the base of a granular layer confined in a Hele-Shaw cell. These oscillations develop in a given range of jet flow-rate, initial granular layer height and grain size. In particular, while the oscillations are fully characterized for $d = 106-212$ μm, no oscillations are observed for the larger grains ($d = 400-600$ μm). Surprisingly, the particle-laden jet oscillates as a solid-body, and a simple metronome model can explain the relationship between its vertical and horizontal frequency, as well as its vertical, horizontal amplitude and jet height. Similar to previous results on the reverse configuration of an impinging jet on the surface of a granular layer in a confined geometry, the Strouhal number displays a power-law behavior but with a larger exponent $\gamma \simeq -5/2$. This points out the possible origin of the self-sustained oscillations in the strong coupling between the fluid and particles. This mechanism could be a possible origin for the periodic behavior which can be exhibited by pockmarks and mud volcanoes in sedimentary basins [43].

ACKNOWLEDGMENTS

The authors acknowledge CNRS for MITI PhD Grant funding. We thank B. Sutherland for interesting discussions, and two anonymous referees for their comments which greatly improved the manuscript.

[1] A. Reusch, M. Loher, D. Bouffard, J. Moernaut, F. Hellmich, F. S. Anselmetti, S. M. Bernasconi, M. Hilbe, A. Kopf, M. D. Lilley, *et al.*, Geophysical Research Letters **42**, 3465 (2015).
[2] A. Gay and S. Migeon, BSGF - Earth Sciences Bulletin **188**, E3 (2017).
[3] M. R. Hudec and J. I. Soto, Basin Research **33**, 2862 (2021).
[4] E. Deville and S. H. Guerlais, Marine and Petroleum Geology **26**, 1681 (2009).
[5] A. Zoporowski and S. A. Miller, Marine and Petroleum Geology **26**, 1879 (2009).
[6] M. P. Dudukovic, F. Larachi, and P. Mills, Catalysis Reviews Science and Engineering **44**, 123 (2002).
[7] V. Makhlin, Theoretical foundations of chemical engineering **43**, 245 (2009).
[8] S. S. E. H. Elnashaie, M. E. Abashar, and F. A. Teymour, Chemical Engineering Science **50**, 49 (1995).
[9] S. Ergun and A. A. Orning, Industrial and Engineering Chemistry **41**, 1179 (1949).
[10] C. Cassar, M. Nicolas, and O. Pouliquen, Physics of fluids **17**, 103301 (2005).
[11] S. Badr, G. Gauthier, and P. Gondret, Physics of Fluids **26**, 023302 (2014).
[12] P. Philippe, P. Cuéllar, F. Brunier-Coulin, L.-H. Luu, N. Benahmed, S. Bonelli, and J.-Y. Delenne, EPJ Web of Conferences **140**, 08014 (2017).
[13] G. Varas, V. Vidal, and J.-C. Géminard, Physical Review E **79**, 021301 (2009).
[14] S. Badr, G. Gauthier, and P. Gondret, Physics of Fluids **28**, 033305 (2016).
[15] P. Aussillous, J. Chauchat, M. Pailha, and M. Médale, Journal of Fluid Mechanics **736**, 594 (2013).
[16] B. Sutherland and S. Dalziel, Physics of Fluids **26**, 035103 (2014).
[17] E. Guazzelli and O. Pouliquen, Journal of Fluid Mechanics **852**, P1 (2018).
[18] A. Carrara, A. Burgisser, and G. W. Bergantz, Journal of Volcanology and Geothermal Research **380**, 19 (2019).
[19] E. C. Bread, J. Dufek, L. Fullard, and A. Carrara, Journal of Geophysical Research Solid Earth **380**, 19 (2019).
[20] S. Gallier, E. Lemaire, F. Peters, and L. Lobry, Journal of Fluid Mechanics **757**, 514 (2014).
[21] G. Gauthier and P. Gondret, Physical Review Fluids **4**, 074308 (2019).
[22] F. Zoueshtiagh and A. Merlen, Physical Review E **75**, 056313 (2007).
[23] P. Philippe and M. Badiane, Physical Review E **87**, 042206 (2013).
[24] X. Cui, J. Li, A. Chan, and D. Chapman, Powder Technology **254**, 299 (2014).
[25] E. P. Montellà, M. Toraldo, B. Chareyre, and L. Sibille, Physical Review E **94**, 052905 (2016).
[26] S. E. Mena, L.-H. Luu, P. Cuéllar, P. Philippe, and J. S. Curtis, AIChE Journal **63**, 1529 (2017).
[27] S. E. Mena, F. Brunier-Coulin, J. S. Curtis, and P. Philippe, Physical Review E **98**, 042902 (2018).
[28] J. Vessaire, G. Varas, S. Joubaud, R. Volk, M. Bourgoin, and V. Vidal, Physical Review Letters **124**, 224502 (2020).
[29] G. Varas, V. Vidal, and J.-C. Géminard, Physical Review E **83**, 011302 (2011).
[30] G. Varas, G. Ramos, J.-C. Géminard, and V. Vidal, Frontiers in Physics **3**, 44 (2015).
[31] See Supplemental Material at [URL will be inserted by publisher] for movie 1, percolation regime [$h_g = 6$ cm, $Q = 3$ mL/min].
[32] See Supplemental Material at [URL will be inserted by publisher] for movie 2, fluidized regime without oscillations [$h_g = 4$ cm, $Q = 15$ mL/min].
[33] See Supplemental Material at [URL will be inserted by publisher] for movie 3, fluidized regime with oscillations [$h_g = 2$ cm, $Q = 35$ mL/min].
[34] O. O. Aderibigde and N. Rajaratnam, Journal of Hydraulic Research **34**, 19 (1996).
[35] D. Rockwell and E. Naudascher, Annual Review of Fluid Mechanics **11**, 67 (1979).
[36] C.-M. Ho and N. S. Nosseir, Journal of Fluid Mechanics **105**, 119 (1981).
[37] E. Villermaux and E. J. Hopfinger, Physica D **72**, 230 (1994).

[38] A. Maurel, P. Ern, B. J. A. Zielinska, and J. E. Wesfreid, Physical Review E **54**, 3643 (1996).
[39] B. W. Righolt, S. Kenjereš, R. Kalter, M. J. Tummers, and C. R. Kleijn, Physics of Fluids **27**, 095107 (2015).
[40] H. Viets, AIAA journal **13**, 1375 (1975).
[41] R. Woszidlo, F. Ostermann, and H.-J. Schmidt, AIAA Journal **57**, 1 (2019).
[42] D. Varieras, P. Brancher, and A. Giovannini, Flow, Turbulence and Combustion **78**, 1 (2007).
[43] F. Girard, J. Sarrazin, and K. Olu, Frontiers in Marine Science **7**, 241 (2020).